Liver International

WILEY

Liver INTERNATIONAL

ORIGINAL ARTICLE OPEN ACCESS

Radiomics-Based Assessment of Portal Hypertension Severity and Risk Stratification of Cirrhotic Patients Using Routine CT Scans

Celine Sin[1,2,3] | Martin Luther Watzenboeck[4,5] | Eugenia Iofinova[1,6] | Lorenz Balcar[5,7,8] | Georg Semmler[5,7] | Bernhard Scheiner[5,7] | Katharina Lampichler[4,5,7] | Mattias Mandorfer[5,7] | Lucile Moga[9,10] | Pierre-Emmanuel Rautou[9,10] | Maxime Ronot[10,11] | Jörg Menche[1,2,3] | Thomas Reiberger[1,5,7,8] | Martina Scharitzer[1,4,5]

[1]CeMM Research Center for Molecular Medicine of the Austrian Academy of Sciences, Vienna, Austria | [2]Max Perutz Labs, Vienna, Austria | [3]University of Vienna, Center for Molecular Biology, Department of Structural and Computational Biology, Vienna, Austria | [4]Department of Biomedical Imaging and Image-Guided Therapy, Medical University of Vienna, Vienna, Austria | [5]Clinical Research Group MOTION, Medical University of Vienna, Vienna, Austria | [6]Institute of Science and Technology Austria, Vienna, Austria | [7]Vienna Hepatic Hemodynamic Laboratory, Division of Gastroenterology and Hepatology, Department of Medicine III, Medical University of Vienna, Vienna, Austria | [8]Christian Doppler Laboratory for Portal Hypertension and Liver Fibrosis, Medical University of Vienna, Vienna, Austria | [9]AP-HP, Hôpital Beaujon, Service d'Hépatologie, DMU DIGEST, Centre de Référence des Maladies Vasculaires du Foie, FILFOIE, ERN RARE-LIVER, Clichy, France | [10]Université Paris-Cité, Inserm, Centre de Recherche sur l'Inflammation, UMR 1149, Paris, France | [11]Service de Radiologie, Hôpital Beaujon, APHP Nord, Clichy & Université Paris Cité, CRI UMR 1149, Paris, France

Correspondence: Martina Scharitzer (martina.scharitzer@meduniwien.ac.at)

Received: 15 June 2025 | **Revised:** 26 February 2026 | **Accepted:** 24 March 2026

Handling Editor: Dr. Alejandro Forner

Keywords: computed tomography | liver | portal hypertension | radiomics | spleen

ABSTRACT

Background & Aims: To develop and validate a CT-based radiomics model to assess HVPG and predict a composite endpoint of liver-related events (LRE: decompensation and liver-related death) in patients with cirrhosis.

Methods: This retrospective study included 357 cirrhosis patients, who received invasive HVPG measurements, 120 liver-healthy controls (training cohort) and 85 and 100 cirrhosis patients (internal and external validation cohorts, respectively), and contrast-enhanced abdominal CTs. After volumetric segmentation of the liver and spleen on CT, Bayesian parameter optimization was used for selection of extracted features and hyperparameter tuning in random forest or elastic net models. Prediction accuracy was evaluated using Pearson correlation coefficients of predicted ('radio-HVPG') and invasive HVPG. Discrimination between relevant HVPG cut-offs was determined by receiver operating characteristic (ROC) analysis. The predictive value of radio-HVPG and invasive-HVPG for LRE was compared using Cox regression models.

Results: Radio-HVPG, predicted by an optimized random forest model based on 74 selected CT features, correlated with invasive-HVPG and detected clinically significant portal hypertension (CSPH: HVPG $\geq$10 mmHg) on the internal (Pearson $r=0.63$, AUC 0.89 [95% CI: 0.81–0.96]) and external (Pearson $r=0.62$, AUC 0.80 [95% CI: 0.64–0.91]) validation cohorts. Radio-HVPG predicted LRE when adjusting for MELD and albumin (adjusted HR: 1.14 [95% CI: 1.04–1.25], $p=0.005$) and performed similarly to invasive-HVPG.

Abbreviations: AIC, Akaike Information Criterion; CRP, C-reactive protein; CSPH, clinically significant portal hypertension; CTP, Child–Turcotte–Pugh score; HCC, hepatocellular carcinoma; HVPG, hepatic venous pressure gradient; INR, international normalized ratio; LRD, liver-related death; MELD, model for end-stage liver disease; PH, portal hypertension.

The first two authors contributed equally to this article.
The last two authors share senior authorship.

Conclusions: Radiomic features accurately predict HVPG in patients with cirrhosis and allow risk stratification for LRE in a radiomics-clinical signature.

1 | Introduction

Portal hypertension (PH), a major consequence of liver cirrhosis, is associated with an increased risk of hepatic decompensation and mortality [1]. Current guidelines recommend invasive measurement of hepatic venous pressure gradient (HVPG) as the reference standard to diagnose portal hypertension [2, 3]. Clinically significant portal hypertension (CSPH), defined by HVPG ≥ 10 mmHg, is linked to a higher risk of hepatic decompensation and mortality [4]. Diagnosing CSPH is crucial as it prompts prophylactic medical therapy in patients with compensated cirrhosis using non-selective beta blockers [5, 6]. Since HVPG measurement is not routinely available in all centres, is minimally invasive, costly, and requires considerable infrastructure and expertise, non-invasive surrogates like serum biomarkers and imaging techniques are being evaluated [7–9]. However, their accuracy in assessing PH severity, predicting outcomes, and monitoring treatment response is limited. Predicting PH severity through CT scans would be particularly advantageous as CT scans are commonly performed in cirrhotic patients to evaluate abdominal symptoms or exclude hepatocellular carcinoma if sonographic vision is restricted [10].

With growing progress in quantitative image analysis, radiomics has evolved as an emerging tool based on converting medical images into quantifiable data. By extracting features in a high-throughput manner, this technique may capture features that are not accessible by the human eye. CT-based studies have shown promising results for personalized diagnosis, treatment decision-making, and clinical prognosis, primarily in the setting of HCC [11]. Additionally, studies have evaluated the performance of radiomics for diagnosing non-alcoholic steatohepatitis [12] and liver fibrosis [13]. In patients with PH, single-slice CT data acquisition for radiomics of the liver has been used due to its less laborious approach compared to complete volumetric liver segmentation [14].

Since a volumetric approach toward radiomics-based CSPH and outcome prediction has not yet been studied, we aimed to develop a radiomics model based on CT-based volumetric segmentation of the liver and spleen to noninvasively assess PH severity and predict clinical outcomes in patients with cirrhosis.

2 | Materials and Methods

2.1 | Study Population

This retrospective study was approved by the institutional review board of our institution (EC number 2180), which waived the requirement for written informed consent. All research was conducted in accordance with the guidelines of the Declarations of Helsinki.

Patients with advanced chronic liver disease (ACLD: i.e., liver stiffness measurement ≥ 10 kPa and/or HVPG ≥ 6 mmHg) undergoing an HVPG measurement at the Hepatic Hemodynamic Lab at the Vienna General Hospital between January 2004 and August 2020, who also underwent an abdominal CT scan within 6 months of the HVPG procedure, were eligible for inclusion. Inclusion criteria were as follows: (1) reliable HVPG measurement, (2) contrast-enhanced CT scans in the portal venous phase with an axial slice thickness of 3 mm. Exclusion criteria were as follows: (i) HCC outside Milan criteria, (ii) previous hepatic surgery, TIPS implantation or splenectomy, (iii) any portal vein thrombosis, or (iv) insufficient CT image quality/data. The study population was split into training ($n = 357$) and validation ($n = 85$, 'internal validation cohort') cohorts with similar distributions of HVPG, age, and sex (Figure 1) using stratified random sampling. To increase the sample size of HVPG < 10 mmHg in the training cohort, consecutive patients without evidence of liver disease (i.e., liver-healthy control group) were included retrospectively. This group consisted of patients undergoing initial abdominal CT for breast or prostate cancer staging, who all had transaminase and liver function parameters in the normal range, with no radiological evidence of hepatic lesions or history of hepatotoxic medication. As HVPG measurements were not available of these patients, HVPG values of 2.5 mmHg were assumed. These patients ($n = 120$) were included exclusively in the training, but not the testing cohort (Figure 1). Details on CT scan acquisition are described in the supplemental material. All patient data were anonymized according to the data management based on our university's ISO 9001:2015 certified quality management system.

2.2 | HVPG Measurement

HVPG measurements were performed according to a published protocol [15] in fasting conditions, using balloon catheters. Only baseline measurements without non-selective beta blockers or nitrate therapy were considered. The HVPG was calculated by subtracting the free from the wedged hepatic venous pressure.

2.3 | External Validation Cohort

An independent validation cohort was acquired from the Beaujon Hospital, Clichy, France ('external validation cohort'). Contrast-enhanced CT scans were acquired during the portal venous phase after intravenous contrast administration in the axial plane with 1.5 mm section thickness reconstruction. One hundred patients were chosen out of a cohort of 228 patients by applying the same inclusion and exclusion criteria from January 2014 until December 2023, randomly selecting 30 patients with an HVPG < 10 mmHg and 70 patients with an HVPG > 9 mmHg.

Lay Summary

We developed and validated a radiomics model based on liver and spleen features, extracted from routine abdominal CT scans, to non-invasively estimate the hepatic venous pressure gradient (HVPG) in patients with chronic liver disease. Our algorithm accurately predicts HVPG both in patients with compensated and decompensated cirrhosis and performs similarly to invasively measured HVPG in identifying patients at risk for hepatic decompensation or liver-related death. Implementing our algorithm in daily clinical practice will allow for more efficient and individualized risk stratification for patients with liver disease, thereby facilitating the early initiation of therapy aiming at the prevention of portal hypertension-related complications and liver-related mortality.

2.4 | Radiomic Feature Extraction, Model Training and Evaluation

Liver and spleen were segmented by a radiologist (15 years of experience in abdominal imaging). Radiomics features were extracted using Pyradiomics v3.0.1 [16]. Feature selection was performed using interfeature correlations and hierarchical clustering, retaining the feature with the highest correlation with HVPG from each cluster. A linear (elastic-net regression) and a tree-based model (random forest regression) were trained to predict HVPG from radiomics features. Bayesian optimization with five-fold cross validation was used for hyperparameter tuning. All feature selection and model optimization steps were performed exclusively in the training cohort.

Prediction accuracy was evaluated using Pearson correlation coefficients and R^2 values of predicted ('radio-HVPG') and true HVPG measurements for both the internal and external validation cohorts. The ability of radio-HVPG to discriminate between clinically relevant HVPG cut-offs was determined by receiver operating characteristic (ROC) analysis. The accuracy of the best-performing model was also evaluated on cACLD patients from the internal validation cohort ($n = 28$).

Additionally, the intraclass correlation coefficient (ICC) for radio-HVPG values based on segmentations from two readers on 25 randomly selected patients of the external validation cohort was calculated.

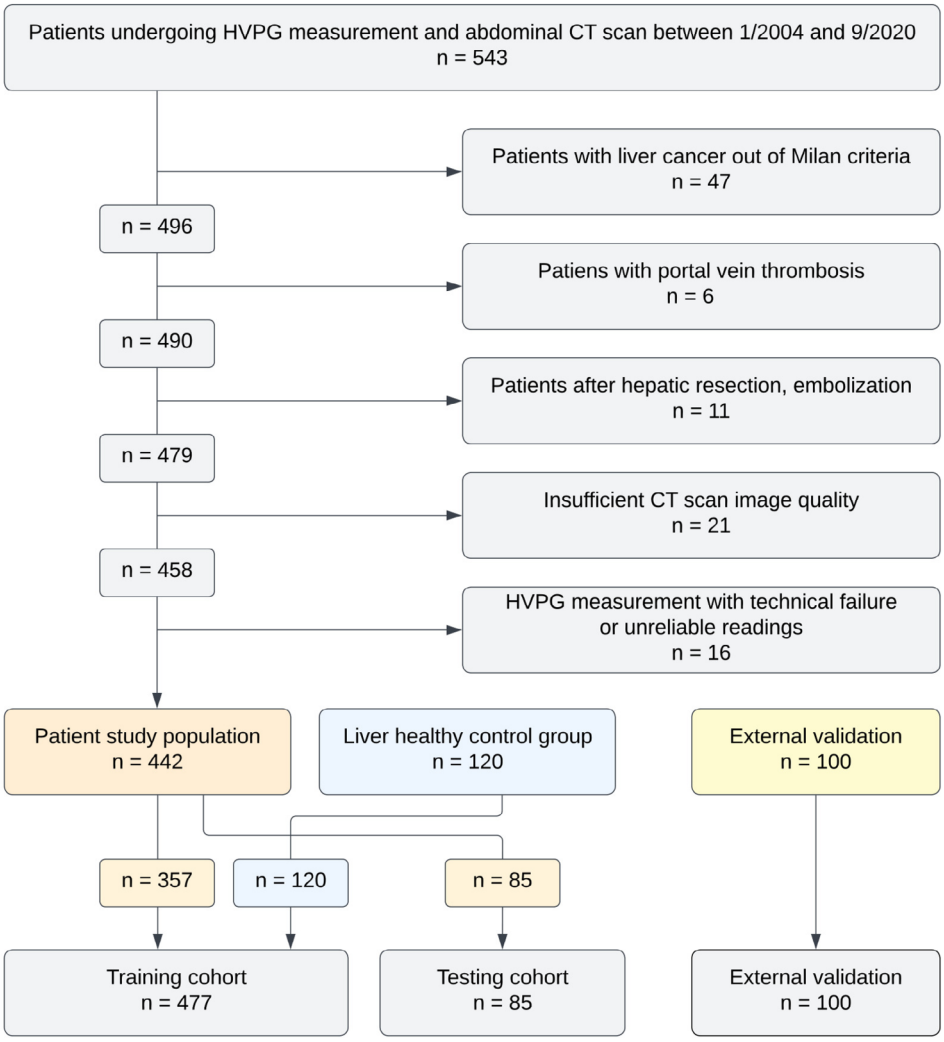

FIGURE 1 | Flowchart shows inclusion and exclusion criteria. HVPG = hepatic venous pressure gradient.

2.5 | Statistics

All statistical analyses were performed using Python 3.7.6 or R 4.2.1 (R Core Team, R Foundation for Statistical Computing). To evaluate the prognostic importance of the radio-HVPG, the composite endpoint liver-related event including first or further hepatic decompensation and liver-related death was assessed in the internal validation cohort. Uni- and multivariable Cox regression analyses were performed to evaluate parameters independently associated with this endpoint. The models were evaluated utilizing radio-HVPG or invasive HVPG measurements, and the performance was compared between these parameters. Additionally, time-dependent multivariable area under the receiver operating characteristic curve (AUROC) analyses were performed in the internal validation cohort to compare the predictive performances of the radio-HVPG versus invasive HVPG for the composite endpoint using marginal weighting at various time points. The level of significance was set at a 2-sided p-value <0.05.

A more detailed description of the feature extraction, model training and evaluation, and statistical analysis steps can be found in the Supporting Information for this manuscript.

3 | Results

3.1 | Patient Characteristics

A total of 442 cirrhotic patients were included in this study (Figure 1). These patients were split into a training ($n=357$; mean age, 58 years ±12 [standard deviation]; 254 men) and a validation cohort (internal validation cohort, $n=85$; mean age, 58 years ±12; 60 men). Median HVPG was 16.5 (IQR 12) mmHg, median Child–Pugh score was 7 (IQR 4) points (Child–Pugh stage A: 45%, B: 39%, C: 16%), and median MELD score was 11 (IQR 8). A total of 330 patients (75%) had CSPH. At baseline, the majority ($n=272$, 61.5%) presented with decompensated liver disease (dACLD), whereas 170 patients (38.5%) were characterized with compensated advanced chronic liver disease (cACLD). Alcoholic liver disease (ALD, $n=184$, 42%) was the predominant aetiology, followed by viral hepatitis ($n=113$, 26%). Indication for CT imaging was HCC screening ($n=209$; 47.3%), assessment for dynamics in portal hypertension ($n=142$; 32.1%), presence of abdominal symptoms ($n=48$; 10.9%), and pre-transplant assessment ($n=19$; 4.3%). In 24 patients (5.4%), the indication of the CT scan could not be ascertained. The median duration between HVPG measurement and abdominal CT examination was 29 days (IQR 67). In the external validation cohort ($n=100$), the median HVPG was 16 (IQR 11) mmHg, median Child–Pugh score was 8 (IQR 4) points, and median MELD score 18 (IQR 8). The median time interval between HVPG measurement and CT examination was 3 days (IQR 26). Further clinical and demographic data are shown in Table 1.

The median follow-up time for the internal validation cohort was 29.5 (95% CI: 20.6–63.5) months. Overall, 35 (41%) patients developed (further) hepatic decompensating events, and 33 (39%) experienced liver-related death. The cumulative incidence of the composite endpoint (decompensation or liver-related death) was 30.7% and 48.3% at 12 and 24 months of follow-up, respectively.

TABLE 1 | Patient characteristics in the training and testing cohorts.

Characteristic	Training cohort	Internal cohort	External cohort
Patients, *n*	357	85	100
Age, years, mean ± SD	57.46 (±11.7)	57.69 (±11.7)	56.8 (±10.6)
Male gender, *n* (%)	254 (71,1%)	60 (70,6%)	63 (63%)
HVPG, *mmHg*, median (IQR)	16 (11)	17 (13)	16 (11)
CSPH, *n* (%)	270 (75,6%)	60 (70,6%)	70 (70%)
Aetiology of liver disease, *n* (%)			
ALD	149 (41,7%)	35 (41,2%)	43 (43%)
NAFLD	40 (11,2%)	5 (5,9%)	11 (11%)
Viral hepatitis	89 (24,9%)	24 (28,2%)	26 (26%)
Other	69 (19,3%)	17 (20%)	14 (14%)
cryptogenic	10 (2,8%)	4 (4,7%)	6 (6%)
Time period between HVPG and CT, *days*, median (IQR)	30 (67)	24 (61)	3 (26)
MELD, *points*, median (IQR)	11 (8)	11 (7)	18 (8)
Child-Pugh score, *points*, median (IQR)	7 (4)	7 (4)	8 (4)
BL-INR, median, (IQR)	1.30 (0.36)	1.31 (0.32)	1.33 (0.45)
BL-albumin, *g/dL*, median (IQR)	35.00 (9.10)	35.70 (9.00)	30.30 (12.00)
BL-bilirubin, *mg/dL*, median (IQR)	1.32 (1.56)	1.48 (1.59)	1.64 (2.11)

Abbreviations: ALD, alcohol-related liver disease; BL, baseline; CSPH, clinically significant portal hypertension; CT, computed tomography; HVPG, hepatic venous pressure gradient; INR, international normalized ratio; MELD, model for end-stage liver disease; NAFLD, non-alcoholic fatty liver disease.

3.2 | Segmentation Reproducibility

Livers and spleens of 25 randomly selected patients from the external validation cohort were segmented by a second rater. Dice similarity coefficients for liver segmentations showed a median of 0.98 (IQR 0.01, range 0.95–0.99), calculated for each reader pair per patient (Figure S1). Similarly, for spleen segmentations, Dice similarity coefficients showed a median of 0.98 (IQR 0.01, range 0.95–0.99). Radio-HVPG calculated based on segmentations by the two raters showed excellent agreement (ICC = 0.98, 95% CI 0.96–0.99).

3.3 | Model Selection and Feature Importance

A total of 2436 features were extracted from the liver and spleen, with 1218 features for each organ. Combined with feature selection algorithm based on hierarchical clustering of Spearman correlation coefficients (Figure 2A), the best random forest regression model outperformed elastic-net regression (Pearson r between predicted and measured HVPG values = 0.7, $R^2 = 0.49$, vs. Pearson $r = 0.6$, $R^2 = 0.36$, Figure S2A-B) on the training data, using five-fold cross validation. In the best performing model, a cut-off of 1.25 was selected for feature clustering, resulting in 74 individual clusters (Figure 2B), from which the feature with the highest Spearman correlation with measured HVPG was selected. These features comprised 34 (45.9%) liver and 40 (54.1%) spleen features. In the subsequently trained random forest regression model, *log−sigma−3−0−mm−3D_glcm_Imc2_spleen*, a Grey Level Co-occurrence Matrix (GLCM, i.e., second-order) feature calculated on spleen voxels, showed the highest feature importance (Figure 2C).

3.4 | Prediction Accuracy in the Internal Validation Cohort

On the internal validation cohort, the HVPG values predicted by the final random forest model (radio-HVPG) correlated with invasive HVPG (Pearson $r = 0.63$, $p < 0.001$, Figure 3A). Radio-HVPG also discriminated well between patients with invasive HVPG greater than or equal to 6 mmHg, i.e., portal hypertension (AUC = 0.89, 95% CI 0.81–0.98, Figure 3B), greater than or equal to 10 mmHg, i.e., CSPH (AUC = 0.86, 95% CI = 0.76–0.95, Figure 3C), greater than or equal to 12 mmHg, i.e., patients at risk of variceal bleeding (AUC = 0.85, 95% CI = 0.76–0.95) and greater than or equal to 16 mmHg (AUC = 0.82, 95% CI = 0.73–0.91). Bland–Altman analysis (Figure S4A) revealed substantial individual-level variability with regards to limits of agreement but no significant bias and no strong systematic trend indicating proportional bias. There was a trend towards underprediction in cases with high HVPG values (≥ 20 mmHg).

Model performance was not significantly impaired when exclusively analysing patients with compensated advanced chronic liver disease in the internal validation cohort. In this patient group, radio-HVPG correlated with invasive HVPG (Pearson $r = 0.66$, $p < 0.001$, Figure S3A), and discriminated between patients with measured HVPG greater than or equal to 6 mmHg (AUC = 0.82, 95% CI 0.65–0.98, Figure S3B), 10 mmHg (AUC = 0.87, 95% CI 0.71–1, Figure S3C), 12 mmHg (AUC = 0.84, 95% CI 0.7–0.99, Figure S3D), and 16 mmHg (AUC = 0.8, 95% CI 0.63–0.98, Figure S3E). Bland–Altman analysis (Figure S4B) revealed substantial individual-level variability with regards to limits of agreement, but no significant bias and no strong systematic trend indicating proportional bias. There was a trend towards underprediction in cases with high HVPG values (≥ 20 mmHg).

3.5 | Prediction Accuracy in the External Validation Cohort

Our model showed similar performance in the external validation cohort. Again, radio-HVPG correlated with measured HVPG (Pearson $r = 0.6$, $p < 0.001$, Figure 4A) and discriminated between patients with measured HVPG greater or equal to 10 mmHg (AUC = 0.78, 95% CI 0.64–91, Figure 4B), 12 mmHg (AUC = 0.8, 95% CI 0.67–0.93, Figure 4C), and 16 mmHg (AUC = 0.79, 95% CI 0.66–0.92, Figure 4D). Bland–Altman analysis (Figure S4C) revealed substantial individual-level variability but no significant bias or major proportional bias. There was a moderately reduced prediction accuracy at higher HVPG values (mean > 15 mmHg).

3.6 | Outcome Prediction

We evaluated the prognostic importance of HVPG assessed by radio-HVPG compared to that derived from invasive HVPG measurement. Upon univariable analysis, radio-HVPG was associated with hepatic decompensation or liver-related death (hazard ratio [HR]: 1.15 per point increase in radio-HVPG [95% CI: 1.06–1.24]; $p < 0.001$). Notably, the independent prognostic value of the radiomics-CSPH group was confirmed in a multivariable model (adjusted HR [aHR]: 1.14 [95% CI: 1.04–1.25]; $p = 0.005$.), adjusted for MELD score and serum albumin (Table 2). In line, invasively measured HVPG was also associated with an increased risk for hepatic decompensation/liver-related death upon univariable (HR: 1.06 per point increase in HVPG [95% CI: 1.02–1.1]; $p < 0.001$) as well as multivariable analyses (aHR: 1.05 [95% CI: 1.01–1.1]; $p = 0.02$; Table 2). Importantly, AIC (264.9873 vs. 268.7195) as well as Concordance index (0.725 ± 0.043 vs. 0.738 ± 0.042) were comparable between models based on radio-HVPG versus the invasively assessed HVPG.

Next, we evaluated whether the presence of clinically significant portal hypertension (CSPH, HVPG ≥ 10 mmHg), based on invasively measured HVPG or radio-HVPG could predict hepatic decompensation/liver-related death. Both invasively measured HVPG (HR: 3.21 [95% CI: 1.24–8.31]; $p = 0.016$; Figure 5A) and radio-HVPG (HR: 3.69 [95% CI: 1.13–12.07]; $p = 0.031$; Figure 5B) were significant predictors of the composite endpoint.

Finally, we compared the predictive performance of the Radiomics-CSPH versus the invasively assessed CSPH for hepatic decompensation/liver-related death in multivariable time-dependent AUROC analyses for the following time points: 12, 24, 36, 48, and 60 months. Notably, time-dependent AUROCs were similar at all evaluated time points using invasive HVPG and radio-HVPG (Figure 5C).

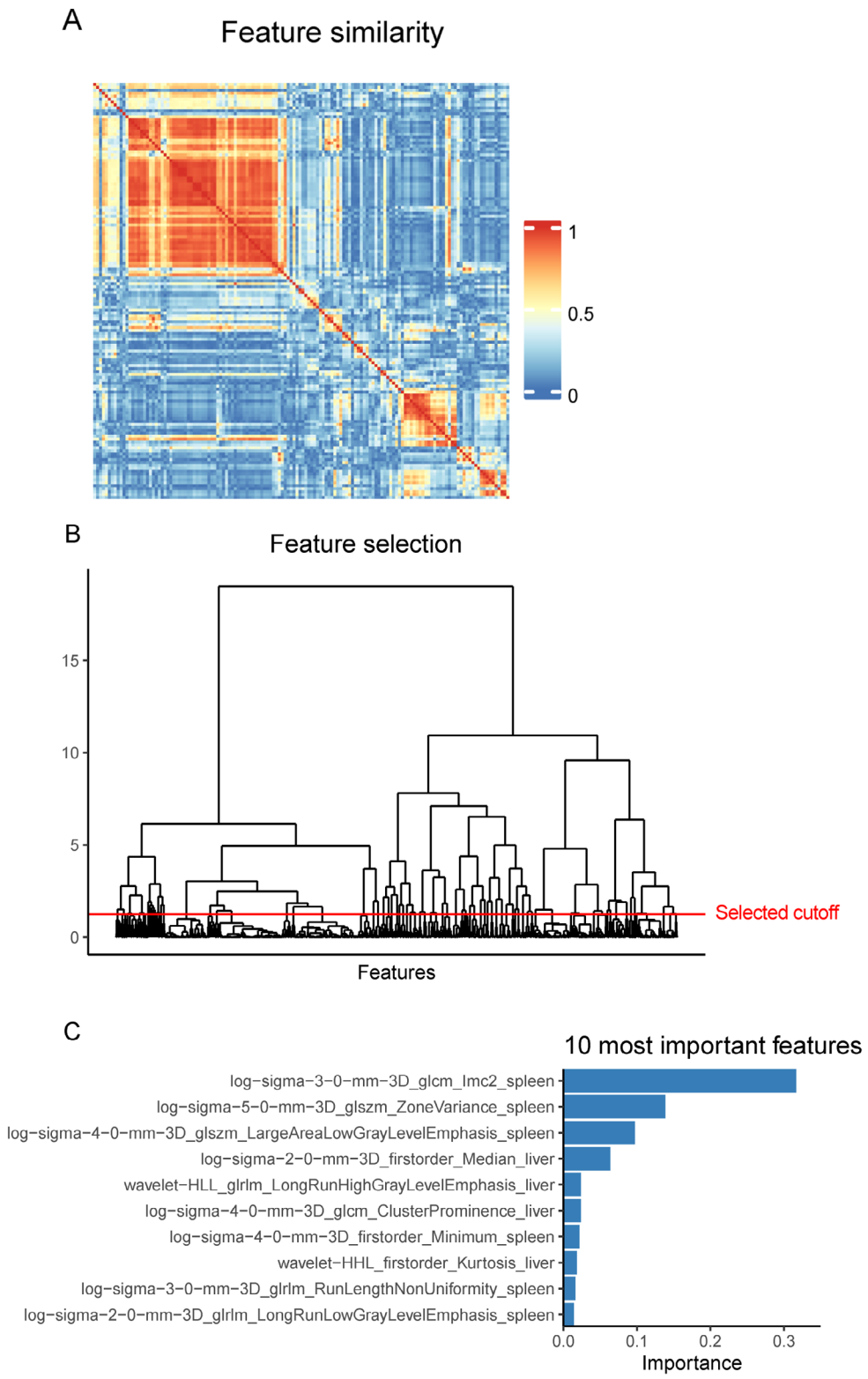

FIGURE 2 | Radiomics feature selection and feature importance. (A) Heatmap showing feature similarity (absolute Spearman correlation), which was used for feature selection and removal of correlated features. (B) Dendrogram showing hierarchical clustering using Ward distances based on feature similarity for feature selection and removal of correlated features prior to random forest training. The selected cutoff height (1.2475) is indicated by the horizontal red line. (C) Feature importance of the 10 most important features in the best performing random forest model.

4 | Discussion

In the present study, we developed a radiomics signature to assess the hepatic venous pressure gradient and predict liver-related outcomes based on volumetric contrast-enhanced CT data. We validated our radiomics signature against the (invasively measured) HVPG as the reference standard within an internal and an external validation cohort. Our radio-HVPG

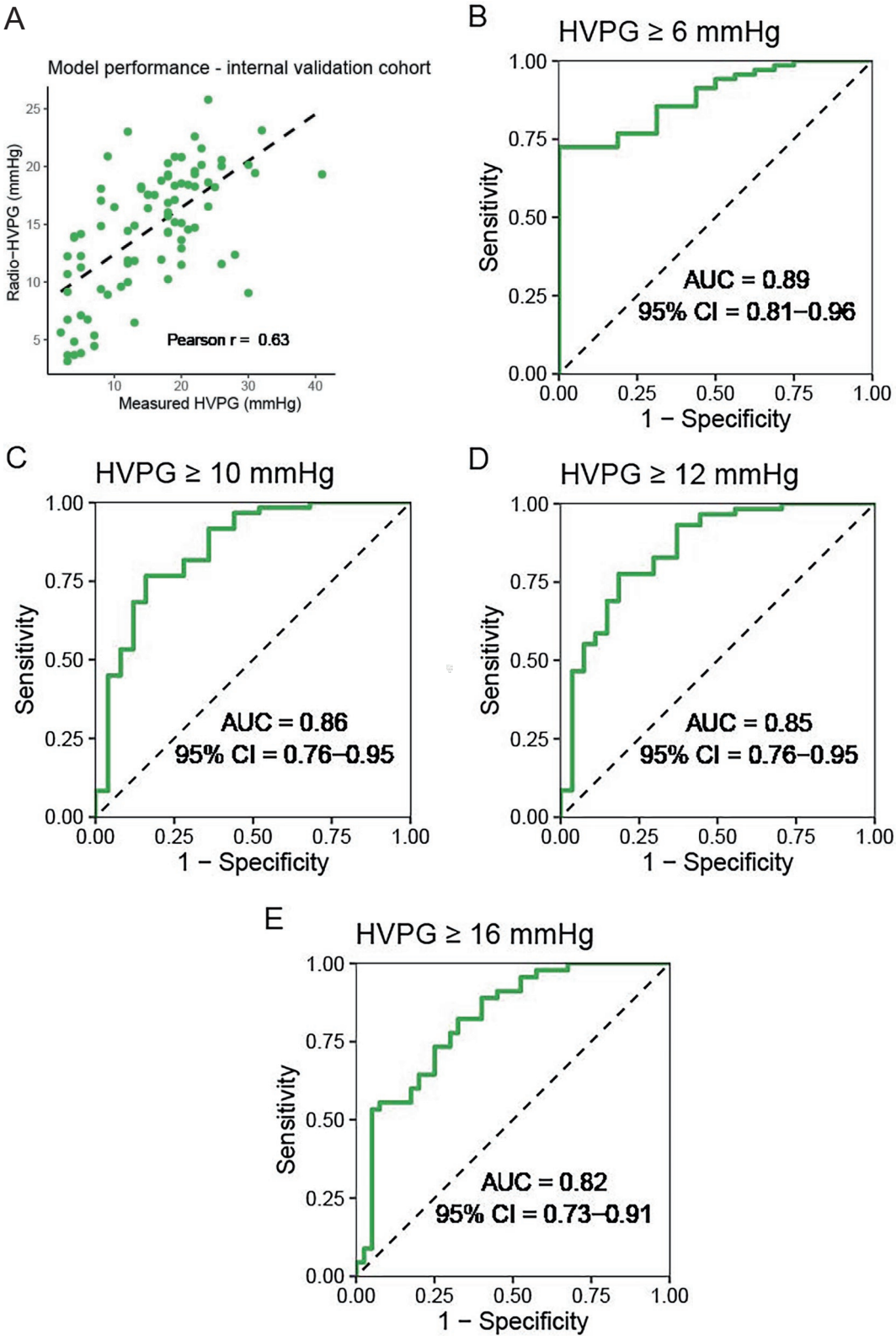

FIGURE 3 | Model performance for the prediction of HVPG on the internal validation cohort. (A) Scatter plot of invasive HVPG and radio-HVPG based on liver and spleen radiomics features. (B-E) AUC curves for discrimination of HVPG ≥ 6 (B), ≥ 10 (C), ≥ 12 (D) and ≥ 16 mmHg (E). HVPG, hepatic venous pressure gradient; AUC, area under the receiver operating characteristic; CI, confidence interval.

model is a random forest regressor using 74 radiomic features chosen for optimal performance—it identified HVPG (Pearson's $r = 0.63$) and CSPH (AUC = 0.86) with high accuracy in an internal cohort and showed robustness in an independent external data set (Pearson's $r = 0.60$, AUC = 0.78). Importantly, the diagnostic performance of radio-HVPG compared to invasive HVPG was confirmed in the internal subgroup of patients with compensated cirrhosis (Pearson $r = 0.66$, $p < 0.001$),

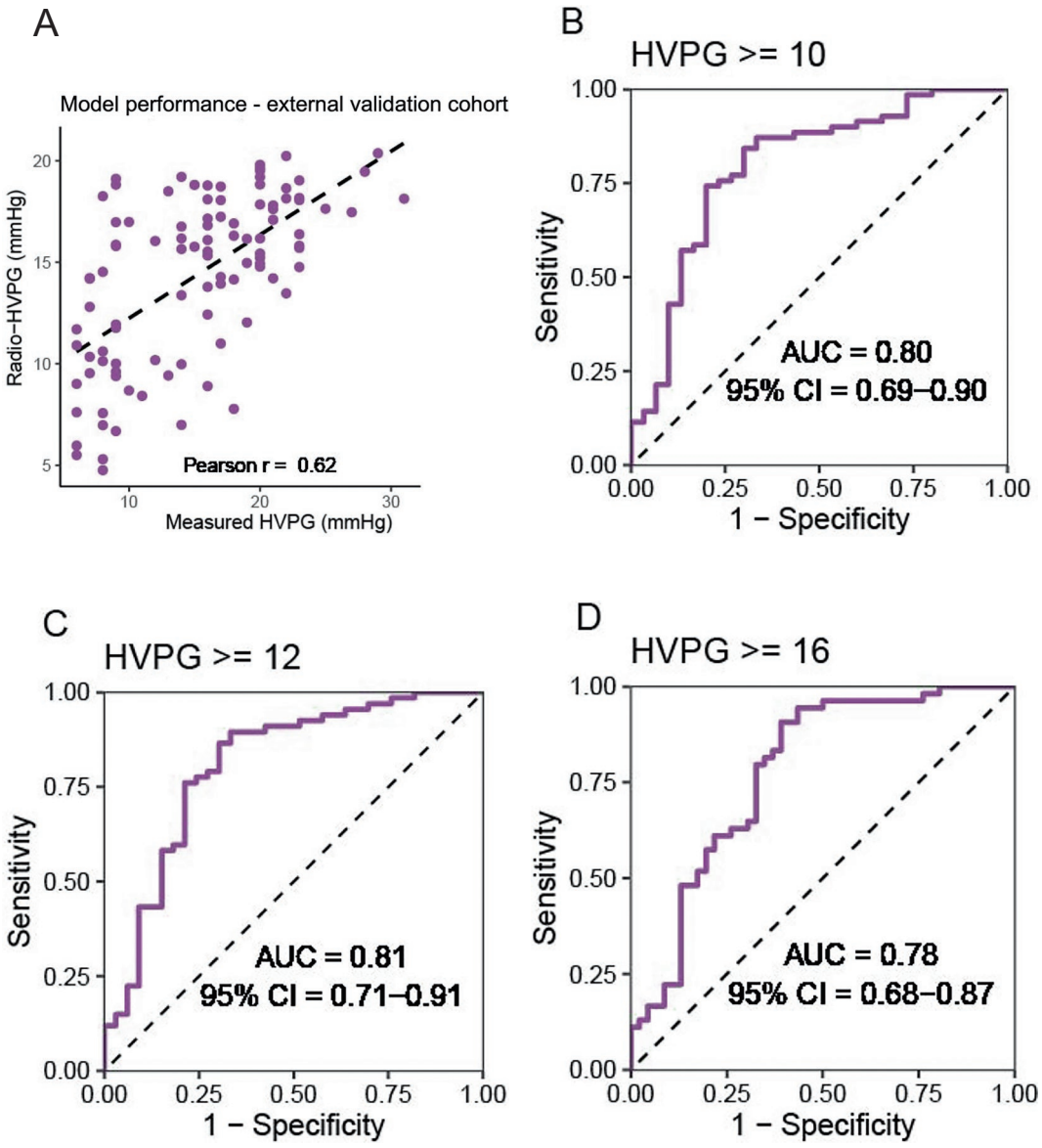

FIGURE 4 | Model performance for the prediction of HVPG on the external validation cohort. (A) Scatter plot of invasive HVPG and radio-HVPG based on liver and spleen radiomics features. (B-D) AUC curves for discrimination of HVPG ≥ 10 (B), ≥ 12 (C), and ≥ 16 mmHg (D). HVPG, hepatic venous pressure gradient.

which is clinically relevant since this enables timely initiation of beta-blocker treatment for prevention of hepatic decompensation [5, 17]. Furthermore, the robustness of radiomics-CSPH for predicting hepatic decompensation or liver-related death was confirmed in a univariable (hazard ratio [HR]: 1.15 per point increase in radio-HVPG [95% CI: 1.06–1.24]; $p < 0.001$) and multivariable model (adjusted HR [aHR]: 1.14 [95% CI: 1.04–1.25]; $p = 0.005$), considering clinical and biochemical factors.

HVPG measurement through hepatic vein catheterization, the gold standard method for assessing portal hypertension severity [2], is invasive and requires substantial resources, specific infrastructure, and expertise. In contrast, CT imaging is widely available and may be indicated in advanced chronic liver disease patients for liver cancer screening [10]. Certain CT findings may hint towards portal hypertension, such as portosystemic collaterals [18] or splenomegaly [19], but with limited specificity. Additionally, liver surface nodularity [20] and other CT features may reflect portal pressure [21], yet these radiological approaches show low diagnostic sensitivity [22] and have not been sufficiently compared to HVPG.

Encouraging results using radiomics and AI-based methods for portal hypertension assessment have been published including 3D hepatic-portal venous reconstruction from CT angiography [13], radiomics signatures from axial single-slice CT images [23], and convolutional neural networks [14, 24]. However, these studies mostly included hepatitis B patients and did not distinguish between those with and without hepatic decompensation, limiting their applicability to Western populations. Given the strong dependence of liver disease progression on aetiology [25] and treatment [26, 27], these findings may not be directly transferrable. Although studies on predicting variceal bleeding [28, 29] and varices recurrence after obliteration exist [30], this study is the first to investigate

TABLE 2 | Factors associated with hepatic decompensation-/liver-related death in the internal validation cohort ($n = 85$).

	Univariable		Radio-HVPG		Invasive HVPG	
Patient characteristics	**HR (95% CI)**	***p***	**aHR (95% CI)**	***p***	**aHR (95% CI)**	***p***
Age (per year)	0.99 (0.97–1.02)	0.57	—		—	
MELD (per point)	1.06 (1.02–1.11)	0.005	0.99 (0.94–1.05)	0.82	1.01 (0.96–1.06)	0.6
CPS (per point)	1.27 (1.14–1.42)	< 0.001	—		—	
Albumin (per g/L)	0.9 (0.86–0.95)	< 0.001	0.91 (0.85–0.97)	0.003	0.92 (0.87–0.98)	0.005
C-reactive protein (per mg/dL)	1.06 (0.97–1.16)	0.18	—		—	
Radio-HVPG	1.15 (1.06–1.24)	< 0.001	1.14 (1.04–1.25)	0.005	—	—
Invasive HVPG	1.06 (1.02–1.1)	< 0.001	—		1.05 (1.01–1.1)	0.021
Model performance						
AIC			264.9873		268.7195	
Concordance index ± SEM			0.738 ± 0.042			

Abbreviations: AHR, adjusted hazard ratio; AIC, Akaike information criterion; CPS, Child–Pugh score; HR, hazard ratio; HVPG, hepatic venous pressure gradient; MELD, model for end-stage liver disease; SEM, standard error of the mean.

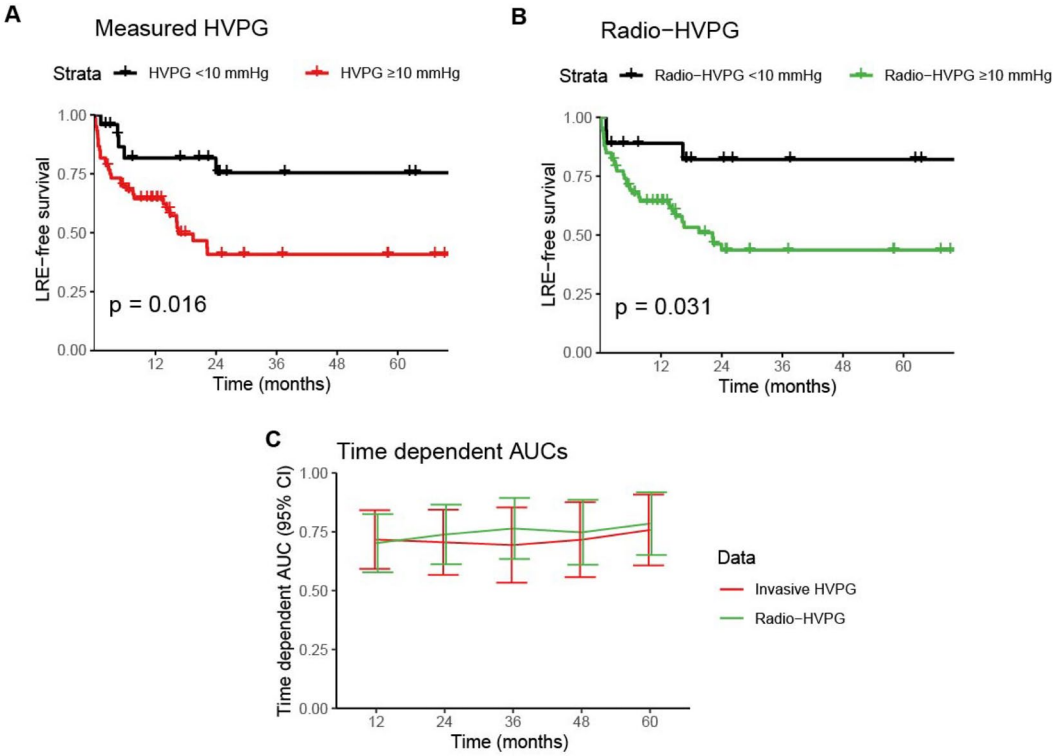

FIGURE 5 | Radio-HVPG predicts liver-related events. Kaplan–Meier curves demonstrating the rate of liver-related events for patients with invasive HVPG (A) or radio-HVPG (B) below or larger than or equal to 10 mmHg, i.e., clinically significant portal hypertension. (C) Time-dependent AUC for the prediction of liver-related events by invasive HVPG or radio-HVPG. HVPG, hepatic venous pressure gradient.

the potential of a CT-based radio-HVPG for predicting hepatic decompensation and liver-related death.

Importantly, radio-HVPG accurately predicted HVPG and provided independent prognostic information, enabling early initiation of betablocker therapy to prevent portal hypertension-related complications and mortality. Its prognostic value was independent of clinically established liver disease severity markers, such as MELD score and albumin, enabling individualized patient management following a combined assessment (MELD, albumin, and CT).

In analysing the best-performing random forest regression model for HVPG prediction, the spleen texture feature, *log–sigma–3–0–mm–3D_glcm_Imc2_spleen*, showed the highest importance in the model by a considerable margin. Considering

that the model had access to shape and texture features from both organs, these data might suggest that portal hypertension correlates with splenic tissue remodelling, which can be quantified using radiomics. This aligns with findings from Sack et al. [31], who observed that texture features were more predictive than size features for cirrhosis in MRI-derived spleen and liver radiomic features. Notably, for our model, the top 10 most important features belonged to the standardized features with excellent reproducibility reported by Zwanenburg et al. [32].

There are limitations to our study: (i) CT images of the external validation cohort were reconstructed with a different slice thickness of 1.5 mm. Although radiomics analysis may depend on volume and voxel number, a large fraction of features has been proven to be robust and stable with varying voxel sizes and slice thickness [33]. We believe the difference in slice thickness most likely accounts for the slight drop in prediction accuracy observed in the external validation cohort. Meanwhile, our radiomics signature, developed on various CT scanners from different manufacturers over several scanner generations, showed robustness on an independent dataset, suggesting our method is independent of image acquisition modality and protocols. (ii) The radiomics approach could be combined with promising laboratory-based machine learning models [34] or elastography-based algorithms [8, 35] to further increase diagnostic and prognostic accuracy. Finally (iii), for model training, in addition to 357 cirrhosis patients with invasively measured HVPG values, 120 liver-healthy controls were included to increase the number of patients with low HVPG values and familiarize the machine learning model with patients without signs of portal hypertension. For these patients, invasively measured HVPG values were not available. Hence, values of 2.5 mmHg were assumed based on the assumption that HVPG values for healthy patients lie between 0 and 5 mmHg [15]. While we acknowledge this assumption may be imprecise in some cases, model evaluation was exclusively performed on patients with invasively measured HVPG.

In conclusion, we developed a non-invasive radiomics tool to predict HVPG in patients with liver disease. Our tool achieved good accuracy in the internal and external testing cohorts as well as in the subset of patients with strictly compensated liver disease, in whom CSPH presence is prognostically and therapeutically of utmost relevance. Furthermore, radio-HVPG predicted the clinical complications of hepatic decompensation or liver-related mortality. Importantly, our radiomics approach is fully based on standard CT imaging that may be indicated for liver cancer screening as the current standard of care. The radio-HVPG will be evaluated in prospective clinical trials.

Author Contributions

Celine Sin: data curation, formal analysis, investigation, methodology, software, visualization, writing – original draft, writing – review and editing. Martin Luther Watzenboeck: formal analysis, methodology, software, visualization, writing – original draft, writing – review and editing. Eugenia Iofinova: conceptualization, software, writing – review and editing. Lorenz Balcar: data curation, formal analysis, visualization, writing – review and editing. Georg Semmler: formal analysis, writing – review and editing. Bernhard Scheiner: data curation, formal analysis, writing – review and editing. Katharina Lampichler: data curation, writing – review and editing. Mattias Mandorfer: writing – review and editing. Lucile Moga: data curation, writing – review and editing. Pierre-Emmanuel Rautou: data curation, writing – review and editing. Maxime Ronot: data curation, writing – review and editing. Jörg Menche: conceptualization, funding acquisition, supervision, writing – review and editing. Thomas Reiberger: conceptualization, investigation, supervision, writing – original draft, writing – review and editing. Martina Scharitzer: conceptualization, data curation, investigation, supervision, methodology, project administration, writing – original draft, writing – review and editing.

Acknowledgements

The computational results presented were partly obtained using the CLIP cluster (https://clip.science/). The authors thank Clemens Watzenboeck from the Medical University of Vienna for the assistance in code upload and repository maintenance. The authors dedicate this work to the memory of Martin Watzenboeck, who served as first author and whose vision and scientific rigor were fundamental to the conception and completion of this study. Open Access funding provided by Medizinische Universitat Wien/KEMÖ.

Funding

This work was supported by the Vienna Science and Technology Fund (WWTF) through projects VRG15-005 and NXT 19-008 granted to J.M and the Clinical Research Group MOTION, Medical University of Vienna, Vienna, Austria – a Clinical Research Group Programme project funded by the Ludwig Boltzmann Gesellschaft (Grant Nr LBG_KFG_22_32) with funds from the Fonds Zukunft Österreich.

P-E.R.'s research laboratory is supported by the Fondation pour la Recherche Médicale (FRM EQU202303016287), "Institut National de la Santé et de la Recherche Médicale" (ATIP AVENIR), the "Agence Nationale de la Recherche" (ANR-18-CE14-0006-01, RHU QUID-NASH, ANR-18-IDEX-0001, ANR-22-CE14-0002) by «Émergence, Ville de Paris», by Fondation ARC, by the European Union's Horizon 2020 research and innovation programme under grant agreement No 847949 and by France 2030 RHU LIVER-TRACK.

Ethics Statement

This retrospective study was approved by the institutional review board of our institution (EC number 2180), which waived the requirement for written informed consent. All research was conducted in accordance with the Declarations of Helsinki.

Conflicts of Interest

M.L.W. has nothing to disclose. C.S. has nothing to disclose. E.I. has nothing to disclose. L.B. has nothing to disclose. G.S. received travel support from Gilead. B.S. received travel support from AbbVie, Ipsen, and Gilead. K.L. has nothing to disclose. M.M. served as a speaker and/or consultant and/or advisory board member for AbbVie, Collective Acumen, Echosens, Gilead, Ipsen, Takeda, and W. L. Gore & Associates and received travel support from AbbVie and Gilead. L.M. has nothing to disclose. P.-E. R. has received research funding from Terrafirma and acted as consultant for Hemostod, Mursla, Genfit, Boehringer Ingelheim and Abbelight, and received speaker fees from Tillots pharma and AbbVie. M.R. received speaker fees from General Electrics, Guerbet, Terumo, Angiodyamics, AstraZeneca, and Servier & consulting fee (to institution) from Quantum Surgical J.M. has nothing to disclose.T.R. received grant support from Abbvie, Boehringer-Ingelheim, Gilead, Intercept, MSD, Myr Pharmaceuticals, Philips Healthcare, Pliant, Siemens and W. L Gore & Associates; speaking honoraria from Abbvie, Gilead, Intercept, Roche, MSD, W. L Gore & Associates; consulting/advisory board fee from Abbvie, Bayer, Boehringer-Ingelheim, Gilead, Intercept, MSD, Siemens; and travel support from Abbvie, Boehringer-Ingelheim, Gilead and Roche. M.S. has nothing to disclose.

Data Availability Statement

Scripts for image processing, extraction of features, feature selection, and model training are available from https://github.com/mlwatzenboeck/RADIPOP and https://github.com/menchelab/radipop_scripts. All other data generated or analyzed during the study are available from the corresponding author by request.

References

1. G. B. D. C. Collaborators, "The Global, Regional, and National Burden of Cirrhosis by Cause in 195 Countries and Territories, 1990-2017: A Systematic Analysis for the Global Burden of Disease Study 2017," *Lancet Gastroenterology & Hepatology* 5 (2020): 245–266.

2. R. de Franchis, J. Bosch, G. Garcia-Tsao, T. Reiberger, C. Ripoll, and V. I. I. F. Baveno, "Baveno VII - Renewing Consensus in Portal Hypertension," *Journal of Hepatology* 76 (2022): 959–974.

3. M. Mandorfer, E. Aigner, M. Cejna, et al., "Austrian Consensus on the Diagnosis and Management of Portal Hypertension in Advanced Chronic Liver Disease (Billroth IV)," *Wiener Klinische Wochenschrift* 135 (2023): 493–523.

4. C. Ripoll, R. Groszmann, G. Garcia-Tsao, and J. S. Barkin, "Hepatic Venous Pressure Gradient Predicts Clinical Decompensation in Patients With Compensated Cirrhosis," *Gastroenterology* 133 (2007): 481–488.

5. C. Villanueva, A. Albillos, J. Genesca, et al., "Beta Blockers to Prevent Decompensation of Cirrhosis in Patients With Clinically Significant Portal Hypertension (PREDESCI): A Randomised, Double-Blind, Placebo-Controlled, Multicentre Trial," *Lancet* 393 (2019): 1597–1608.

6. T. Reiberger, G. Ulbrich, A. Ferlitsch, et al., "Carvedilol for Primary Prophylaxis of Variceal Bleeding in Cirrhotic Patients With Haemodynamic Non-Response to Propranolol," *Gut* 62 (2013): 1634–1641.

7. M. Mandorfer, V. Hernandez-Gea, J. C. Garcia-Pagan, and T. Reiberger, "Noninvasive Diagnostics for Portal Hypertension: A Comprehensive Review," *Seminars in Liver Disease* 40 (2020): 240–255.

8. T. Reiberger, "The Value of Liver and Spleen Stiffness for Evaluation of Portal Hypertension in Compensated Cirrhosis," *Hepatol Commun* 6 (2022): 950–964.

9. E. Dajti, F. Ravaioli, R. Zykus, et al., "Accuracy of Spleen Stiffness Measurement for the Diagnosis of Clinically Significant Portal Hypertension in Patients With Compensated Advanced Chronic Liver Disease: A Systematic Review and Individual Patient Data Meta-Analysis," *Lancet Gastroenterology & Hepatology* 8 (2023): 816–828.

10. European Association for the Study of the Liver. Electronic address eee, European Association for the Study of the L, "EASL Clinical Practice Guidelines: Management of Hepatocellular Carcinoma," *Journal of Hepatology* 69 (2018): 182–236.

11. J. Wei, H. Jiang, D. Gu, et al., "Radiomics in Liver Diseases: Current Progress and Future Opportunities," *Liver International* 40 (2020): 2050–2063.

12. S. Naganawa, K. Enooku, R. Tateishi, et al., "Imaging Prediction of Nonalcoholic Steatohepatitis Using Computed Tomography Texture Analysis," *European Radiology* 28 (2018): 3050–3058.

13. K. J. Choi, J. K. Jang, S. S. Lee, et al., "Development and Validation of a Deep Learning System for Staging Liver Fibrosis by Using Contrast Agent-Enhanced CT Images in the Liver," *Radiology* 289 (2018): 688–697.

14. Y. Liu, Z. Ning, N. Ormeci, et al., "Deep Convolutional Neural Network-Aided Detection of Portal Hypertension in Patients With Cirrhosis," *Clinical Gastroenterology and Hepatology* 18 (2020): 2998–3007.

15. T. Reiberger, P. Schwabl, M. Trauner, M. Peck-Radosavljevic, and M. Mandorfer, "Measurement of the Hepatic Venous Pressure Gradient and Transjugular Liver Biopsy," *Journal of Visualized Experiments* (2020), https://doi.org/10.3791/58819.

16. J. J. M. van Griethuysen, A. Fedorov, C. Parmar, et al., "Computational Radiomics System to Decode the Radiographic Phenotype," *Cancer Research* 77 (2017): e104–e107.

17. C. Villanueva, F. Torres, S. K. Sarin, et al., "Carvedilol Reduces the Risk of Decompensation and Mortality in Patients With Compensated Cirrhosis in a Competing-Risk Meta-Analysis," *Journal of Hepatology* 77 (2022): 1014–1025.

18. M. Simon-Talero, D. Roccarina, J. Martinez, et al., "Association Between Portosystemic Shunts and Increased Complications and Mortality in Patients With Cirrhosis," *Gastroenterology* 154 (2018): 1694–1705.

19. N. Bastati, L. Beer, A. Ba-Ssalamah, et al., "Gadoxetic Acid-Enhanced MRI-Derived Functional Liver Imaging Score (FLIS) and Spleen Diameter Predict Outcomes in ACLD," *Journal of Hepatology* 77 (2022): 1005–1013.

20. R. Sartoris, P. E. Rautou, L. Elkrief, et al., "Quantification of Liver Surface Nodularity at CT: Utility for Detection of Portal Hypertension," *Radiology* 289 (2018): 698–707.

21. P. Iranmanesh, O. Vazquez, S. Terraz, et al., "Accurate Computed Tomography-Based Portal Pressure Assessment in Patients With Hepatocellular Carcinoma," *Journal of Hepatology* 60 (2014): 969–974.

22. B. Procopet and A. Berzigotti, "Diagnosis of Cirrhosis and Portal Hypertension: Imaging, Non-Invasive Markers of Fibrosis and Liver Biopsy," *Gastroenterol Rep (Oxf)* 5 (2017): 79–89.

23. F. Liu, Z. Ning, Y. Liu, et al., "Development and Validation of a Radiomics Signature for Clinically Significant Portal Hypertension in Cirrhosis (CHESS1701): A Prospective Multicenter Study," *eBioMedicine* 36 (2018): 151–158.

24. Q. Yu, Y. Huang, X. Li, et al., "An Imaging-Based Artificial Intelligence Model for Non-Invasive Grading of Hepatic Venous Pressure Gradient in Cirrhotic Portal Hypertension," *Cell Reports Medicine* 3 (2022): 100563.

25. P. Konigshofer, B. S. Hofer, K. Brusilovskaya, et al., "Distinct Structural and Dynamic Components of Portal Hypertension in Different Animal Models and Human Liver Disease Etiologies," *Hepatology* 75 (2022): 610–622.

26. G. Semmler, T. Binter, K. Kozbial, et al., "Noninvasive Risk Stratification After HCV Eradication in Patients With Advanced Chronic Liver Disease," *Hepatology* 73 (2021): 1275–1289.

27. B. S. Hofer, B. Simbrunner, L. Hartl, et al., "Alcohol Abstinence Improves Prognosis Across All Stages of Portal Hypertension in Alcohol-Related Cirrhosis," *Clinical Gastroenterology and Hepatology* 21 (2023): 2308–2317.

28. S. Wan, Y. Wei, H. Yu, Y. Li, S. Yao, and B. Song, "Computed Tomographic Portography With Esophageal Variceal Measurements in the Evaluation of Esophageal Variceal Severity and Assessment of Esophageal Variceal Volume Efficacy," *Academic Radiology* 27 (2020): 528–535.

29. X. Yan, Z. Leng, Q. Xu, Z. Zhang, M. Xu, and J. Li, "The Influences of Timing of Urgent Endoscopy in Patients With Acute Variceal Bleeding: A Cohort Study," *BMC Gastroenterology* 22 (2022): 506.

30. Y. Tseng, L. Ma, S. Li, et al., "Application of CT-Based Radiomics in Predicting Portal Pressure and Patient Outcome in Portal Hypertension," *European Journal of Radiology* 126 (2020): 108927.

31. J. Sack, J. Nitsch, H. Meine, R. Kikinis, M. Halle, and A. Rutherford, "Quantitative Analysis of Liver Disease Using MRI-Based Radiomic Features of the Liver and Spleen," *J Imaging* 8 (2022): 277.

32. A. Zwanenburg, M. Vallieres, M. A. Abdalah, et al., "The Image Biomarker Standardization Initiative: Standardized Quantitative Radiomics for High-Throughput Image-Based Phenotyping," *Radiology* 295 (2020): 328–338.

33. L. Escudero Sanchez, L. Rundo, A. B. Gill, M. Hoare, E. Mendes Serrao, and E. Sala, "Robustness of Radiomic Features in CT Images With Different Slice Thickness, Comparing Liver Tumour and Muscle," *Scientific Reports* 11 (2021): 8262.

34. J. Reinis, O. Petrenko, B. Simbrunner, et al., "Assessment of Portal Hypertension Severity Using Machine Learning Models in Patients With Compensated Cirrhosis," *Journal of Hepatology* 78 (2023): 390–400.

35. M. Pons, S. Augustin, B. Scheiner, et al., "Noninvasive Diagnosis of Portal Hypertension in Patients With Compensated Advanced Chronic Liver Disease," *American Journal of Gastroenterology* 116 (2021): 723–732.

Supporting Information

Additional supporting information can be found online in the Supporting Information section. **Figure S1:** Reproducibility of segmentations and radio-HVPG by a second rater. (A) Boxplots indicating mean, interquartile range, and range of pairwise inter-observer Dice similarity coefficients for liver and spleen segmentations. (B) Scatter plot radio-HVPG values based on liver and spleen segmentations by the two raters. **Figure S2:** Comparison of linear and tree-based regression models for prediction of HVPG. Scatter plots of invasive HVPG and radio-HVPG (predicted based on liver and spleen radiomics features) using random forest regression (A) or elastic-net regression (B). **Figure S3:** Model performance for the prediction of HVPG on patients compensated at baseline in the internal validation cohort. (A) Scatter plot of invasive HVPG and radio-HVPG of patients with compensated cirrhosis. (B-E) AUC curves for discrimination of HVPG ≥ 6 (B), ≥ 10 (C), ≥ 12 (D), and ≥ 16 mmHg (E). **Figure S4:** Bland–Altman analysis of model performance across validation cohorts. Bland–Altman plots illustrating agreement between predicted and observed values for (A) the internal validation cohort, corresponding to the regression analysis presented in Figure 3; (B) the compensated patient subset, corresponding to Figure S3; and (C) the external validation cohort, corresponding to Figure 4. For each cohort, Bland–Altman analyses were systematically cross-referenced with their respective regression plots to comprehensively assess model agreement and identify potential systematic bias.